Trion Electroluminescence from Semiconducting Carbon Nanotubes

Florian Jakubka, Stefan B. Grimm, Yuriy Zakharko, Florentina Gannott, and Jana Zaumseil*

Department of Materials Science and Engineering, Friedrich-Alexander-Universität Erlangen-Nürnberg, 91058 Erlangen, Germany

ABSTRACT Near-infrared emission from semiconducting single-walled carbon nanotubes (SWNTs) usually results from radiative relaxation of excitons. By binding an additional electron or hole through chemical or electrochemical doping, charged three-body excitons, so-called trions, are created that emit light at lower energies. The energy difference is large enough to observe weak trion photoluminescence from doped SWNTs even at room temperature. Here, we demonstrate strong trion electroluminescence from electrolyte-gated, light-emitting SWNT transistors with three different polymer-sorted carbon nanotube species, namely, (6,5), (7,5) and (10,5). The red-shifted trion emission is equal to or even stronger than the exciton emission, which is attributed to the high charge carrier density in the transistor channel. The possibility of trions as a radiative relaxation pathway for triplets and dark excitons that are formed in large numbers by electron–hole recombination is discussed. The ratio of trion to exciton emission can be tuned by the applied voltages, enabling voltage-controlled near-infrared light sources with narrow line widths that are solution-processable and operate at low voltages (<3 V).

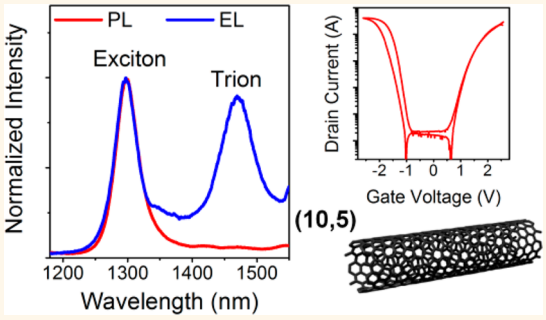

KEYWORDS: trion · carbon nanotubes · electrolyte gating · transistor · near-infrared · electroluminescence

Near-infrared light emission from semiconducting single-walled carbon nanotubes (SWNTs) results from radiative relaxation of excitons.[1] These bound electron–hole pairs are created by absorption of light (photoluminescence, PL) or recombination of electrically injected holes and electrons (electroluminescence, EL).[2,3] The emission wavelengths are directly determined by the chirality vector (*n*,*m*) and therefore bandgap of the nanotubes. Emission line widths are usually narrow (<50 meV) even at room temperature. Binding of an additional electron or hole creates charged three-body excitons (X^-, X^+) analogous to H^- or H_2^+, respectively.[4,5] These charged exciton species are elementary quasi-particles named trions that are lower in energy than the corresponding neutral excitons. Trions have recently attracted a lot of attention in single layer transition metal dichalcogenides (TMDs)[6−8] but were studied in semiconductor quantum wells for some time due to their extra charge and nonzero spin.[5,9,10] However, while trions in TMDs and semiconductor quantum wells are only clearly observable at low temperatures, trions in semiconducting SWNT created by chemical[11−13] or electrochemical doping[14] are detectable in photoluminescence spectra at room temperature due to the short-range Coulomb interaction in these one-dimensional systems and thus large energy separation (100–200 meV). Here, we show that trion electroluminescence from semiconducting SWNT at high charge carrier densities is comparable to or even stronger than exciton emission from the same device. We demonstrate this effect for three different, nearly single-species semiconducting carbon nanotube networks in ambipolar, electrolyte-gated, light-emitting transistors. The exciton and trion peaks are well-resolved with narrow line widths of less than 70 nm. Depending on the applied voltages the ratio of trion to exciton emission can be tuned, forming a type of voltage-controlled emitter in the near-infrared. The large carrier concentrations that are accumulated by electrolyte-gating and the conversion of dark excitons and triplets into emissive trions are discussed as the possible origin of this effect.

RESULTS AND DISCUSSION

Three different semiconducting SWNT species, namely (6,5), (7,5) and (10,5), were selected by dispersion with polyfluorene copolymers as introduced by Nish *et al.*[15] and enriched by sedimentation and redispersion

* Address correspondence to jana.zaumseil@fau.de.

Received for review June 5, 2014 and accepted July 15, 2014.

Published online July 16, 2014
10.1021/nn503046y

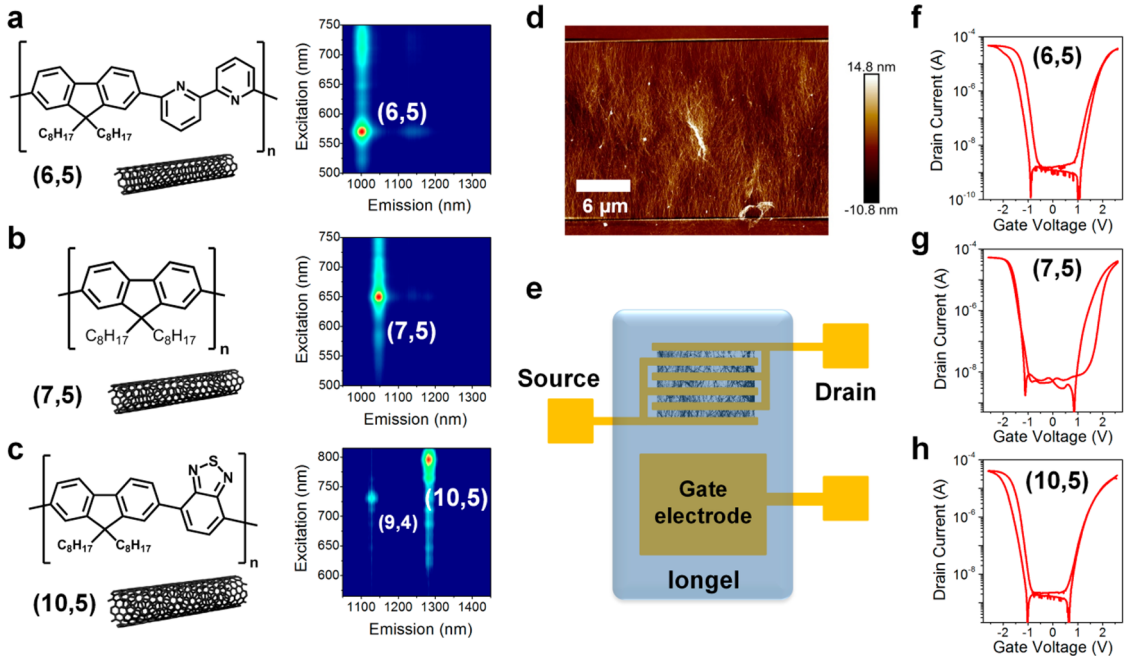

Figure 1. (a–c) Molecular structures of conjugated polymers used for selective dispersion of (6,5), (7,5) and (10,5) SWNTs and respective PL maps of the enriched dispersions. (d) AFM image of dense, aligned SWNT network between source and drain electrodes (channel length $L = 20\ \mu m$). (e) Schematic illustration of an electrolyte-gated transistor (top view) with ionogel and side-gate electrode. (f–h) Transfer characteristics at low source-drain voltages ($V_{ds} = -0.01$ V) for electrolyte-gated transistors based on (6,5), (7,5) and (10,5) SWNT networks, respectively.

as described previously.[3,16] Figure 1a–c shows the polymers, respective nanotube species and photoluminescence maps of the SWNT dispersions that were used for device fabrication. All photoluminescence maps exhibit only one main emission peak, which corresponds to the (6,5), (7,5) and (10,5) nanotubes, respectively, and confirms the high selectivity of the sorting process. Dropcasting these dispersions under an applied electric field and removal of residual polymer by washing with tetrahydrofuran yielded aligned and dense networks of nanotubes, as shown in Figure 1d. Instead of conventional backgating or top gating with an oxide or polymer dielectric these SWNT networks were gated *via* an ionogel based on an ionic liquid ([EMIM][FAP]) and a fluorinated polymer (P(VDF-HFP)).[17] The ionogel acts as an electrolyte with a wide electrochemical window. When a gate voltage is applied the anions and cations move to the gate electrode and semiconductor, respectively, and form electric double layers. Because the applied gate voltage drops over these nm-thick ionic layers the effective capacitance is very large (few $\mu F \cdot cm^{-2}$) and therefore enables very efficient gating and the accumulation of large charge carrier densities. These electrolyte-gated transistors (EGTs) operate at voltages of less than 3 V.[18] The efficient gating also leads to improved ambipolar charge injection due to quasi-transparent injection barriers for both holes and electrons.[19,20] SWNT-EGTs have the additional advantage of being very robust against surface roughness, sample imperfections and even allow for stretchable devices.[21] Moreover, due to the underlying mechanism of ion diffusion and formation of electric double layers the gate electrode does not need to be on top of the channel but can be located quite far away (side-gate geometry) as shown in the schematic illustration of the employed device geometry (Figure 1e).

All SWNT-EGTs show clear ambipolar transfer characteristics with high on/off current ratios ($10^5 - 10^6$) for low source-drain voltages (−10 mV) and clear onsets for hole accumulation and electron accumulation (Figure 1f–h). Because of the density and alignment of the nanotubes the maximum estimated charge carrier mobilities are high for both holes (8–15 $cm^2\ V^{-1}\ s^{-1}$) and electrons (3–8 $cm^2\ V^{-1}\ s^{-1}$). The voltage gap between the onset voltages for hole transport and electron transport can in principle be used to determine the bandgap of carbon nanotubes. However, due to the potential drop between the gate electrode and the source electrode the applied gate voltage is offset from the real electrochemical potential, whose determination would require an additional reference electrode.[22,23] Nevertheless, the onset voltage gap for the (6,5) nanotubes is 1.94 V and that for the (10,5) nanotubes is 1.66 V and thus follows the expected bandgap difference of 0.277 eV between the two nanotubes (E_{11}(6,5) = 1.270 eV, E_{11}(10,5) = 0.993 eV)[24] very well.

Ambipolar transistors, independent of the semiconducting material, show characteristic V-shaped transfer curves that shift with the applied source-drain voltages (V_{ds}), due to the change of potential difference between the drain and gate electrode.[25] This behavior is

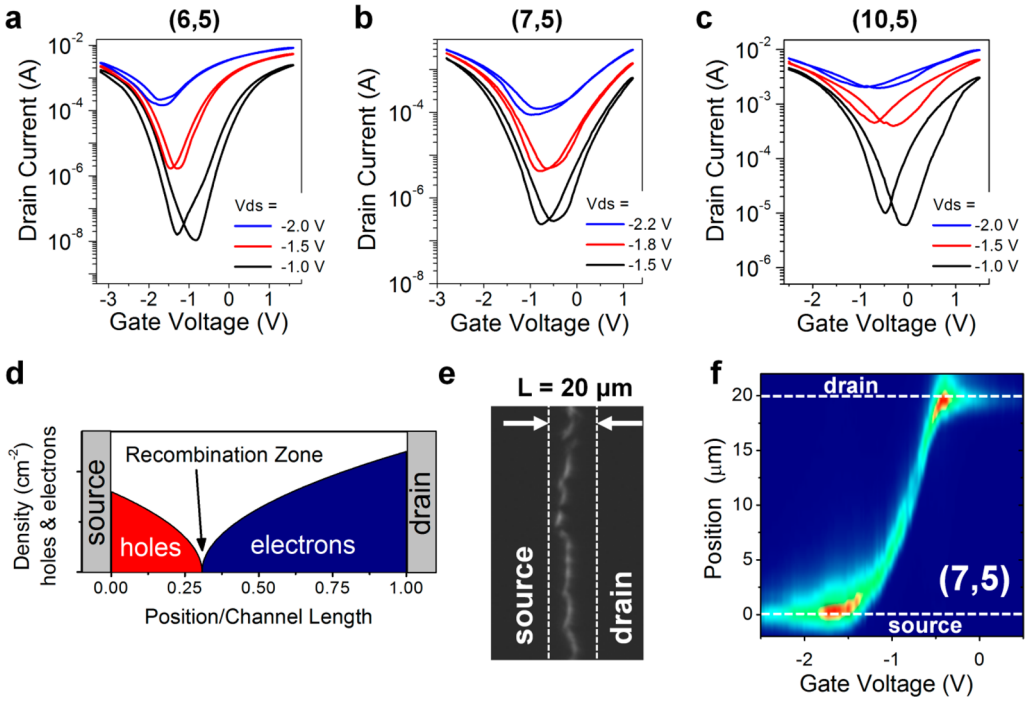

Figure 2. (a–c) Transfer characteristics for (6,5), (7,5) and (10,5) SWNT-EGTs at high source-drain voltages (−1 to −2 V) indicating ambipolar transport. (d) Schematic illustration of hole and electron accumulation and recombination zone for a transistor in the ambipolar regime. (e) Near-infrared image (wavelengths 800–1600 nm) of the recombination and emission zone in a (7,5) SWNT-EGT in the ambipolar regime. (f) Position (distance from source electrode) and intensity of emission depending on gate voltage (V_{ds} = −2 V) for the same device.

also observed for SWNT-EGTs as shown in Figure 2a–c. For source-drain voltages of −1 to −2 V the transition from unipolar electron accumulation (low positive gate voltage) *via* the ambipolar regime (low negative gate voltages) to the unipolar hole accumulation regime (high negative gate voltage) is observed for all three nanotube networks. In the ambipolar regime a hole accumulation layer and an electron accumulation layer are formed simultaneously that meet within the channel (see Figure 2d). At this point electron–hole recombination and thus light emission take place similar to previously demonstrated light-emitting transistors based on organic semiconductors,[26,27] carbon nanotubes[2,3] and TMDs.[28,29] This recombination and emission zone is shown for a (7,5) SWNT-EGT in Figure 2e. Its apparent width of about 2 μm is mainly limited by the resolution of the optical setup. The emission zone is not perfectly straight, which is due to density variations of the carbon nanotube network. The position of the recombination zone within the channel is directly determined by the applied voltages as shown for a transistor with (7,5) nanotubes in Figure 2f (see also Supporting Information, Figure S1).

Semiconducting carbon nanotubes show electroluminescence in the near-infrared depending on their diameter. For ambipolar light-emitting SWNT transistors with conventional gate dielectrics the electroluminescence spectra correspond to the photoluminescence spectra of the respective nanotubes as shown for ambipolar SWNT transistors in a top-gate geometry with a polymer dielectric[3] (see also Supporting Information, Figure S2). For electrolyte-gated light-emitting transistors this is not the case. Figure 3 presents the PL and EL spectra of SWNT-EGTs with different SWNT species. All EL spectra show strong additional peaks at lower energies compared to the PL spectra of the neutral SWNT networks at the same spot. Photoluminescence features at those wavelengths have recently been attributed to several different states, such as oxygen-induced defects,[30] local zero-dimension-like states generated by oxygen doping,[31] symmetry-breaking sp^3-defects[32] and trions.[11,14] Since our nanotube films were processed in dry nitrogen before encapsulation, were dispersed by noncovalent polymer-wrapping and do exhibit only weak D-peaks in their Raman spectra (see Supporting Information, Figure S3) we assume that defect-induced emission can be neglected. We therefore propose that the observed red-shifted EL peaks are due to positively or negatively charged trions.

To confirm this notion we acquired photoluminescence spectra (see Figure 4) from the channel region under constant laser excitation at different positive (electron accumulation) and negative (hole accumulation) gate voltages with the source and drain electrodes at ground potential. For both hole and electron accumulation the exciton emission sharply decreased until it completely vanished (see also Figure S4, Supporting Information). This behavior can be used to determine the oxidation and reduction potentials of carbon nanotubes.[22,23] Charge-induced Auger-type quenching

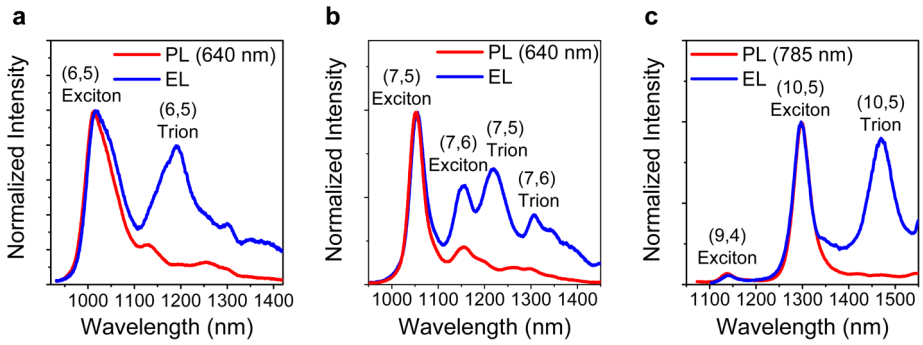

Figure 3. (a–c) Photoluminescence and electroluminescence spectra from EGTs with (6,5), (7,5) and (10,5) SWNTs, respectively. Note, the (6,5) SWNT network also contains small amounts of (7,5) nanotubes and the network of (7,5) nanotubes contains some (7,6) nanotubes. Because of efficient charge and excitation transfer within the aligned and dense network emission from (7,5) at 1052 nm and from (7,6) nanotubes at 1152 nm, respectively, is visible in both the PL and EL spectra.

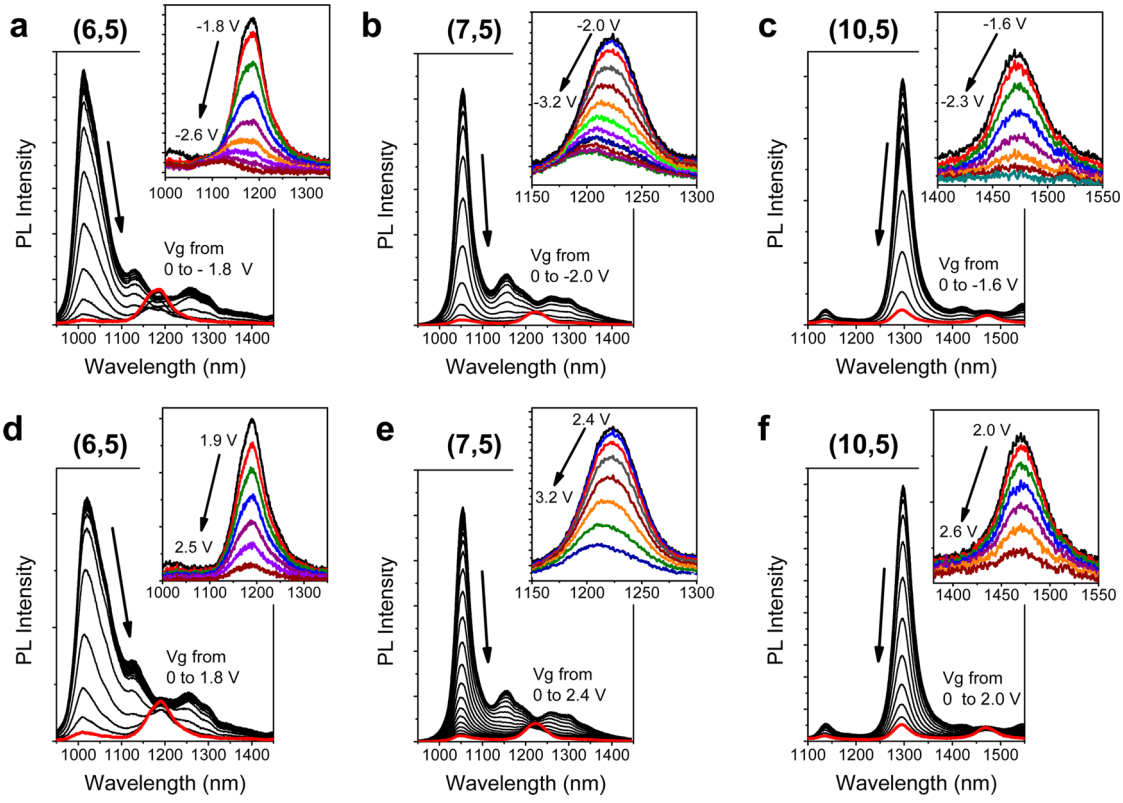

Figure 4. Evolution of PL spectra from neutral to strong hole doping (a–c) and strong electron doping (d–f) of (6,5), (7,5) and (10,5) SWNT networks, respectively. The red curve indicates the maximum intensity of trion emission. The insets show the decrease and shift of trion emission for further increasing positive or negative gate voltage.

as well as the reduction of the absorption cross section for the E_{22} transition are assumed to be the origin.[33] While the exciton emission faded a second peak appeared for all nanotube species at lower energies for high doping levels. The appearance and disappearance of this peak was completely reversible and only depended on the applied gate voltage. Therefore, we exclude any possible creation of covalent defects and identify the observed peak as emission from positively or negatively charged trions. The positive and negative trion peak energies are very similar, which is expected due to the nearly equal effective masses of holes and electrons in carbon nanotubes.[14] The energy difference ΔE between the observed exciton and trion emission is equal to about 176 meV for (6,5), 165 meV for (7,5) and 114 meV for (10,5) nanotubes (see also Table 1). These values are consistent with the model for trion emission by Matsunaga *et al.*[11] and Park *et al.*[14] who estimated ΔE as the sum of the exchange splitting energy that scales with $1/d^2$ and the trion binding energy that scales with $1/d$ as shown in Figure 5. The trion peaks reached their maximum when the exciton emission was already strongly quenched (see Supporting Information, Figure S4). With further increasing positive or negative gate voltages the

TABLE 1. Summary of Observed Exciton and Trion Emission Wavelengths, Energies and Energy Differences (ΔE)

	(6,5)	(7,5)	(10,5)
exciton	1019 nm (1.217 eV)	1052 nm (1.178 eV)	1296 nm (0.957 eV)
trion$^+$	1184 nm (1.047 eV)	1224 nm (1.013 eV)	1473 nm (0.842 eV)
trion$^-$	1191 nm (1.041 eV)	1224 nm (1.013 eV)	1471 nm (0.843 eV)
ΔE trion$^+$	170 meV	165 meV	115 meV
ΔE trion$^-$	176 meV	165 meV	114 meV

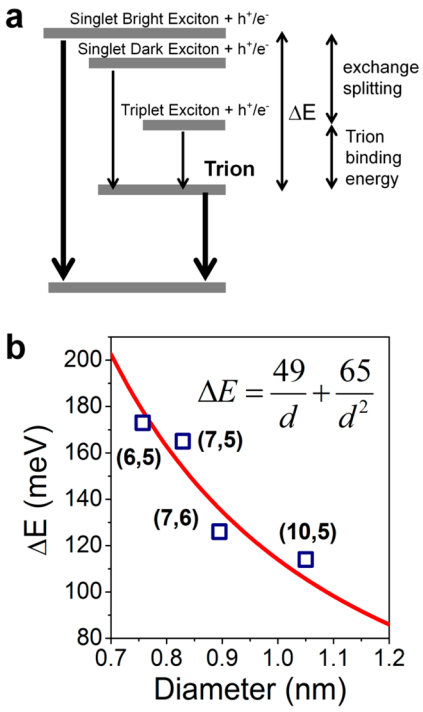

Figure 5. (a) Schematic energy diagram of bright and dark excitons and trions in semiconducting SWNT. (b) Energy difference between trions and excitons for four different SWNT species (squares) compared to theoretical dependence (red line) according to Park *et al.*[14]

intensity of the trion emission reduced again. Increased Auger quenching and reduction of the E_{22} absorption are probably the reason for this decrease. The trion peaks also showed a blue-shift with gate voltage. Although a dependence of the emission energy of a charged excited state on electric field or doping level might be expected, it is not clear, why the emission shifts to higher energies. A likely reason for the blue-shift of the trion emission could be a decrease of the trion binding energy with doping. For excitons Spataru *et al.* predicted a blue-shift of the E_{11} transition due to a strong decrease of the exciton binding energy with doping.[34] This would be consistent with the observation that the blue-shift is strongest for the (6,5) nanotubes, which also have the largest trion binding energy of the three investigated nanotubes species.

Although the observed peaks in the PL spectra of the different carbon nanotube networks were previously associated with trion emission and fit the expected diameter dependence we cannot completely exclude the possibility of emission from unintentional sp^3-defects (see discussion on defect emission above) that only become observable when the dominant exciton emission is quenched. However, gate voltage dependent absorption spectra (Figure 6) of the transistor channels for hole and electron doping provide additional evidence that we indeed observe trions. Accumulation of holes or electrons initially leads to a reduction of the E_{11} absorption, which is expected for electrochemical or chemical doping of nanotubes.[11,20] For networks with more than one nanotube species (see Figure 6c,f) a clear dependence of absorption bleaching on the diameter of the respective nanotubes is observed. Importantly, we also find increased absorption at the wavelengths corresponding to trion absorption for moderate hole and electron accumulation. These weak absorption peaks disappear again when the gate voltage is increased further and the first subband is completely filled or emptied. The detailed dependence of trion absorption and E_{11} bleaching on gate voltage is shown in Figure S5 (Supporting Information).

The PL and absorption spectra of hole and electron doped nanotube networks confirm that the spectral features of the EL spectra for electrolyte-gated SWNT transistors can be assigned to trion emission in addition to exciton emission. As shown above trions are formed by excitons in the presence of excess holes or electrons. The strong trion electroluminescence suggests that either the emission zone within the ambipolar EGTs cannot be seen as intrinsic with zero charge carrier density as proposed for some organic light-emitting transistors,[27] or charges penetrate the accumulation layers of opposite charge polarity and recombine there. Because of the limited spatial resolution in the near-infrared it is not possible to determine whether trion emission mainly occurs at the edges of the emission zone or equally from the center. Because of the similar energies of positively and negatively charged trions it is also impossible to determine whether one type dominates in the EL.

Further, relatively large carrier densities have to be accumulated to obtain similar exciton to trion emission ratios for PL as for EL in the same device. For example, in the case of the (10,5) nanotubes gate voltages of 0.6 to 1 V above the onset voltage have to be applied in order to reach equal exciton and trion photoluminescence (see Figures 3c and 4c). The charge carrier density within the channel of an ideal ambipolar transistor can be calculated as shown in Figure S6 (Supporting Information). It is much lower near the recombination zone, where the EL originates, than the values calculated for uniform charge accumulation in the same device at the gate voltages used in the PL quenching experiments. The strong trion emission observed in the EL spectra suggests that trions are not only created by the combination of a bright singlet exciton and a charge as

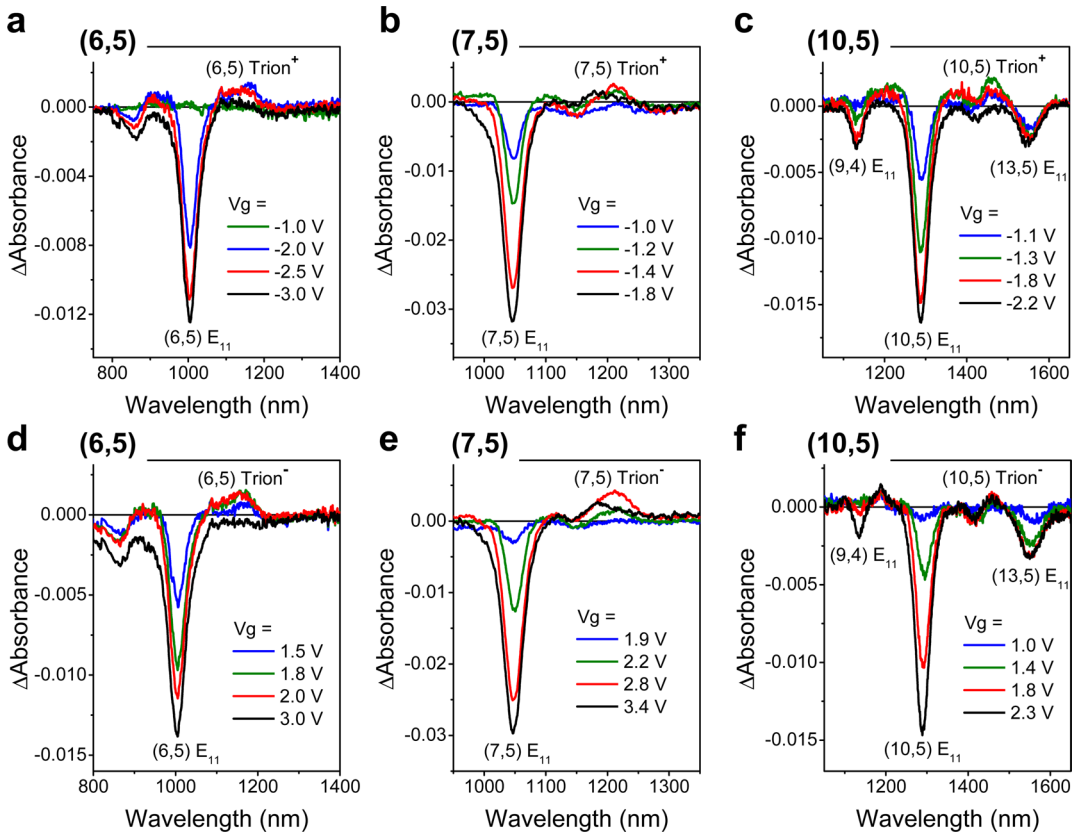

Figure 6. Change of absorbance from neutral to strong hole doping (a–c) and strong electron doping (d–f) for (6,5), (7,5) and (10,5) SWNT networks, respectively, indicating ground state bleaching (decrease of E_{11} transition) and doping-induced trion absorption.

in the PL spectra, but additional trion formation takes place. Bright trions might be created from dark excitons[13] or triplet excitons.[35] These nonemissive states are generated in large numbers by electron–hole recombination in carbon nanotubes, which has been suggested as one of the reasons for the low EL efficiencies in electroluminescent SWNT devices.[36] Formation of trions could thus be a possible pathway for turning nonemissive species into emissive species, although at an energy cost, *i.e.*, emission at longer wavelengths. The strong trion emission in the EL-spectra compared to the PL-spectra could thus be explained by the conversion of dark excitons and triplets into bright trions.

The difference between the EL spectra from electrolyte-gated (strong trion emission) and conventionally gated (no trion emission) SWNT networks (see also Figure S2, Supporting Information) may be explained by the different charge carrier densities within the channel. Typical carrier densities in a field-effect transistor with a polymer or oxide gate dielectric are on the order of 10^{12} cm^{-2}. In contrast to that, the accumulated hole and electron densities in electrolyte-gated transistors are one to 2 orders of magnitude higher and can reach 10^{14} cm^{-2}. For SWNT-EGTs hole and electron densities of about 0.5 charges per nm were estimated.[20] Given that the exciton diffusion length in nanotubes was estimated to be up to 200 nm,[37] the probability that an exciton encounters a hole or electron before radiative or nonradiative decay is extremely high for electrolyte-gated SWNT networks and thus the probability of Auger quenching and trion formation should be high as well.

If trion emission depends on the charge carrier density within the channel it should be controllable. Figure 7 shows the evolution of the EL spectra of all three types of SWNT-EGTs depending on the applied source-drain voltages. In all cases the overall intensity of the EL increases and the ratio of trion to exciton emission shifts clearly in favor of trion emission. In the case of the (10,5) nanotubes the trion emission even starts to dominate over the exciton emission. The simple model for the local potential and charge carrier density distribution within an ambipolar transistor (see Supporting Information Figure S6) shows that the electric field within the recombination zone and the carrier density in its direct vicinity are increased substantially by increasing the source-drain bias. Both would enhance the probability of trion formation due to the escape of carriers into the oppositely charged accumulation layer and thus exciton formation amid an excess of holes or electrons. The tunability of the ratio of exciton to trion emission could also be utilized to create voltage-controlled two-wavelengths emitters.

Because of the alignment of the nanotubes during deposition the emitted light is strongly polarized

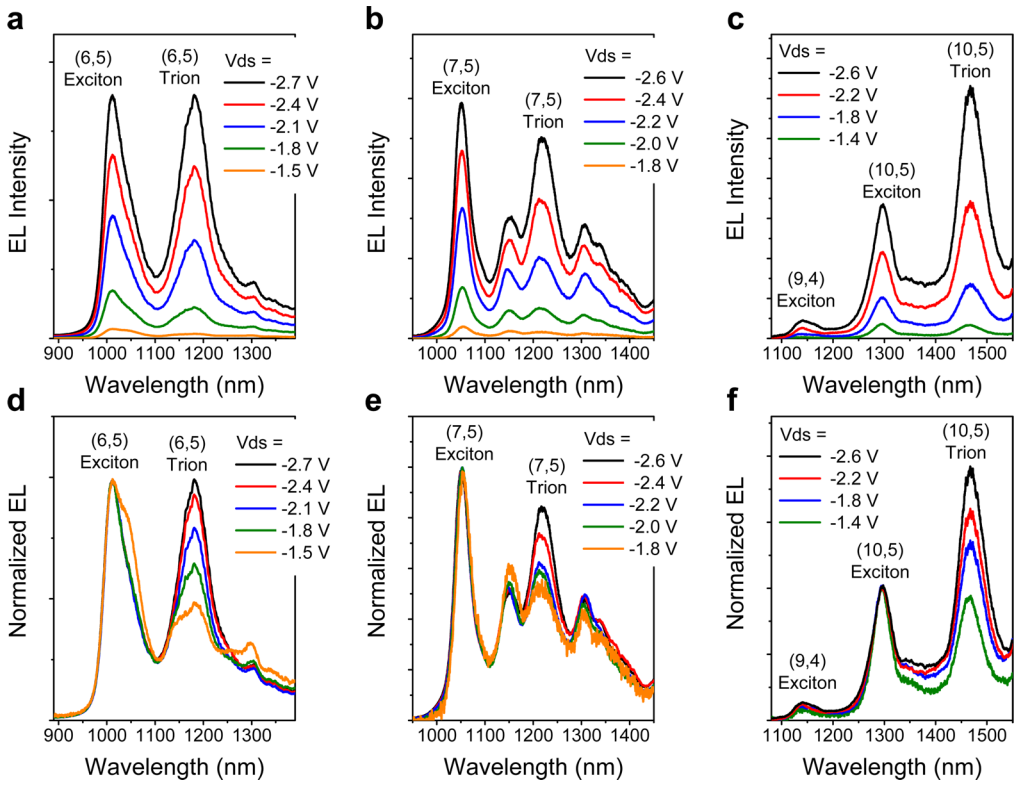

Figure 7. (a–c) EL spectra of (6,5), (7,5) and (10,5) SWNT-EGTs, respectively for different source-drain voltages (V_{ds}) and (d–f) corresponding normalized spectra showing the increase of trion emission with source-drain voltage compared to the exciton emission.

parallel to the charge transport direction as shown in Figure 8a for an EGT with aligned (10,5) nanotubes and with an EL intensity ratio ($I_{\parallel}/I_{\perp}$) of 5, which corresponds to a degree of polarization, defined as $(I_{\parallel} - I_{\perp})/(I_{\parallel} + I_{\perp})$ of 67%. The peak intensities of exciton as well as trion emission follow the $\cos^2$ dependence (Figure 8b) as expected for well-aligned dipole emitters.

For potential applications of light-emitting SWNT-EGTs their brightness and efficiency are important. Our devices emit about 1–20 nW of near-infrared light (see Supporting Information, Figure S7) from a total pixel area of about 0.01 cm^2 (active emission area 0.0004 cm^2). This corresponds to an estimated external quantum efficiency of about 10^{-6} to10^{-5} photons per injected electron These values are an order of magnitude lower than for conventionally gated light-emitting SWNT transistors[3] and suggest that strong Auger quenching overall reduces radiative decay in these devices. Although the EL efficiencies are low compared to current commercial near-infrared LEDs based on InGaAsP heterostructures (see Supporting Information, Figure S8) the large current densities (~500 A/cm^2) at low voltages (<3 V) enabled by electrolyte-gating generate sufficient optical output for applications where high brightness is less important than solution-processability and flexibility.

Considering possible applications the (10,5) SWNT-EGTs are especially interesting. Their narrow exciton peak at 1297 nm (full width at half-maximum (fwhm) of 42 nm, *i.e.*, 31 meV) lies within the O-band for

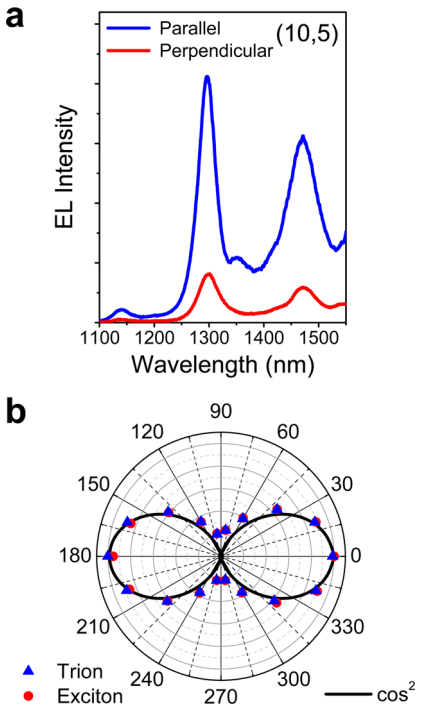

Figure 8. (a) EL spectra of a (10,5) SWNT-EGT for parallel and perpendicular orientation of a linear polarization filter with respect to charge transport direction. (b) Dependence of normalized peak intensity for exciton and trion emission on polarization angle.

telecommunication and the second biological transparency window.[38,39] InGaAsP light-emitting diodes

fabricated by planar epitaxial technology exhibit line width of 70 to 100 nm. The trion peak at 1471 nm (fwhm of 74 nm, *i.e.*, 42 meV) is close to one of the absorption peaks of oxygenated blood. The possibility to tune the ratio of these two emission peaks by simply changing the applied voltages and the robustness of the electrolyte-gating technique against variations of substrate topography (*e.g.*, due to a waveguide) could be useful for a range of diagnostic and sensor applications.

CONCLUSION

In summary, we have demonstrated strong trion electroluminescence from electrolyte-gated carbon nanotube transistors that operate at low voltages. Trion emission is a direct result of the high charge carrier densities in electrolyte-gated transistors. The formation of trions might be a possible pathway to convert dark excitons and triplets that are generated by electron–hole recombination into emissive species, while Auger-quenching of exciton emission reduces the overall efficiency in these devices. The trion to exciton emission ratio can be tuned by the applied source-drain bias. This tunability, narrow line widths of both emission peaks in the near-infrared, linear polarization of the emitted light and the simplicity of device fabrication are promising features for potential applications.

METHODS

Materials. CoMoCat single-walled carbon nanotubes (Aldrich, diameter 0.7–0.9 nm), HipCO single-walled carbon nanotubes (Unidym Inc., batch P2172, diameter 0.8–1.2 nm, <11 wt % iron), poly(9,9-dioctylfluorene) (PFO, Aldrich, M_w = 75 kg·mol^{-1}, PD = 3.4), poly(9,9-dioctylfluorene-*co*-benzothiadiazole) (F8BT, American Dye Source, M_w = 164 kg·mol^{-1}, PD = 4.1), poly[(9,9-dioctylfluorenyl-2,7-diyl)-*alt*-co-(6,6′-(2,2′-bipyridine))] (PFO-BPy, American Dye Source, M_w = 76 kg·mol^{-1}, PD = 2.8), ionic liquid 1-ethyl-3-methyl-imidazolium tris(pentafluoroethyl)-trifluorophosphate ([EMIM][FAP], high purity grade, Merck), and poly(vinylidene fluoride-*co*-hexafluoropropylene) (P(VDF-HFP), Aldrich, M_w ∼ 400 kg·mol^{-1}, M_n ∼ 130 kg·mol^{-1}) were all used as received without further purification.

Selection and Purification of SWNTs. 15 mg of nanotube powder (CoMoCat for (6,5) and (7,5) nanotubes and HipCO for (10,5) nanotubes) were dispersed in 10 mL of a 3 mg·mL^{-1} solution of conjugated polymer (PFO-BPy for (6,5) SWNT, PFO for (7,5) SWNT and F8BT for (10,5) SWNT) in toluene and bath sonicated for 90 min. The resulting dispersion was centrifuged at 74200*g* for 45 min (Beckman Coulter Avanti J26XP). The supernatant was further ultracentrifuged at 268000*g* for 60 min to remove any remaining bundles and then for 12 h at 268000*g* to sediment the majority of the nanotubes (Beckman Coulter OptimaMax XP table top centrifuge with a swinging bucket rotor MLS-50, thick-walled polyallomer tubes). The SWNT pellet that was formed at the bottom of the centrifuge tube was washed several times with toluene to remove residual polymer and then redispered in toluene by mild bath sonication. Photoluminescence excitation–emission maps were collected with a Horiba Jobin-Yvon Fluorolog-3 spectrometer with a Symphony-II InGaAs diode array detector.

Devices Fabrication. Interdigitated source/drain electrodes (channel width W = 20 mm, channel length L = 20 μm) were patterned on thin glass substrates (Schott AF32 Eco, thickness 300 μm) by photolithography (double layer photoresist LOR5B/S1813), electron-beam evaporation of 2 nm chromium and 30 nm gold, and lift-off. For aligned SWNT thin films, the enriched SWNT dispersions without free polymer were dropcast twice (10 μL) onto hot substrates (100 °C) while a bias of 50 to 100 V was applied between the source/drain electrodes during the first dropcasting step and the reverse voltage during the second step. After SWNT deposition the substrates were washed with tetrahydrofuran and isopropanol to remove any residual polymer, polyallomer and large aggregates. Tapping-mode atomic force microscopy (AFM) images were obtained with a Veeco diDimension 5000 AFM. The nanotube networks were annealed in dry nitrogen atmosphere at 290 °C for 30 min to remove adsorbed water and oxygen. The iongel was spin-coated on top at 2000 rpm from a solution of [EMIM][FAP]:P(VDF-HFP):acetone (4:1:14 by mass) and excess iongel around the device was removed with acetone. Annealing in nitrogen at 80 °C for several hours removed any residual solvent. All devices were encapsulated with a piece of glass and Delo Katiobond LP655 resin to allow for measurements in air. Current–voltage characteristics of the electrolyte-gated transistors were recorded with an Agilent 4155C semiconductor parameter analyzer or a Keithley 2612A source-meter. All measurements were performed at room temperature.

Optical Measurements. EL images were recorded with a thermoelectrically cooled 256 × 360 pixel InGaAs camera (Xenics XEVA-CL-TE3, sensitivity range: 800–1600 nm). PL and EL spectra were obtained with an Acton SpectraPro SP2358 spectrometer (grating 150 lines/mm) and a liquid nitrogen cooled InGaAs line camera (PI Acton OMA V:1024 1.7). For PL measurements a 640 nm laser diode and a 785 nm laser diode (OBIS, Coherent Europe B.V.) were used. The laser beam was defocused onto the substrate through the collecting near-infrared objective (×50, N.A. 0.65, with correction for glass thickness) to illuminate an area of about 100 μm in diameter. Power densities varied from 50 to 200 W/cm^2. A cold mirror (875 nm) and an additional long-pass filter (850 nm) were used to reject visible and scattered laser light. For current–voltage-luminance measurements a calibrated InGaAs photodiode (Thorlabs FGA21-CAL, active area 3.1 mm^2) was placed directly underneath the device (active area ∼1 mm^2) to collect as much of the emitted light as possible. The photocurrent was recorded at 0 V bias. Calculations of the optical power and external quantum efficiency took the observed electroluminescence spectrum and wavelength dependent sensitivity of the photodiode into account. Gate voltage dependent absorption spectra were recorded on the same device geometry using a Varian Cary 6000i absorption spectrometer and restricting the light beam to the active transistor area with an aperture of 1 mm in diameter. The absorption spectrum of the device at a gate voltage, for which neither holes nor electrons were accumulated, served as the baseline and the change of absorbance was obtained for hole and electron accumulation at negative and positive gate voltages, respectively.

Conflict of Interest: The authors declare no competing financial interest.

Acknowledgment. This research was funded by the Deutsche Forschungsgemeinschaft (DFG) *via* the Collaborative Research Center "Synthetic Carbon Allotropes" (SFB 953). F.J. acknowledges support by the DFG (Grant ZA 638/3) and the Erlangen Graduate School in Advanced Optical Technologies (SAOT, GSC 80). J.Z. also acknowledges general support by the Alfried Krupp von Bohlen und Halbach-Stiftung *via* the "Alfried Krupp Förderpreis für junge Hochschullehrer" and the Cluster of Excellence "Engineering of Advanced Materials" (EXC 315). The authors thank Udo Mundloch and the Institute of Advanced Materials and Processes (ZMP Fürth) for help with ultracentrifugation and photoluminescence measurements.

Supporting Information Available: Drain current and position of emission zone *vs* gate voltage for a (7,5) SWNT-EGT, transfer characteristics and emission spectra of top-gate SWNT

transistors with PMMA dielectric, Raman spectra of the SWNT films in the device, peak intensities of exciton emission and trion emission *vs* gate voltage, evolution of absorption spectra of SWNT networks *vs* gate voltage, calculated distribution of charge carrier density within the channel of an ambipolar transistor, optical output *vs* gate voltage for three EGTs, comparison between SWNT-EGTs and commercial near-infrared LEDs. This material is available free of charge *via* the Internet at http://pubs.acs.org.

REFERENCES AND NOTES

1. Wang, F.; Dukovic, G.; Brus, L. E.; Heinz, T. F. The Optical Resonances in Carbon Nanotubes Arise from Excitons. *Science* **2005**, *308*, 838–841.
2. Freitag, M.; Chen, J.; Tersoff, J.; Tsang, J. C.; Fu, Q.; Liu, J.; Avouris, P. Mobile Ambipolar Domain in Carbon-Nanotube Infrared Emitters. *Phys. Rev. Lett.* **2004**, *93*, 076803.
3. Jakubka, F.; Backes, C.; Gannott, F.; Mundloch, U.; Hauke, F.; Hirsch, A.; Zaumseil, J. Mapping Charge Transport by Electroluminescence in Chirality-Selected Carbon Nanotube Networks. *ACS Nano* **2013**, *7*, 7428–7435.
4. Lampert, M. A. Mobile and Immobile Effective-Mass-Particle Complexes in Nonmetallic Solids. *Phys. Rev. Lett.* **1958**, *1*, 450–453.
5. Finkelstein, G.; Shtrikman, H.; Bar-Joseph, I. Negatively and Positively Charged Excitons in GaAs/$Al_xGa_{1-x}As$ Quantum Wells. *Phys. Rev. B: Condens. Matter Mater. Phys.* **1996**, *53*, R1709–R1712.
6. Mak, K. F.; He, K.; Lee, C.; Lee, G. H.; Hone, J.; Heinz, T. F.; Shan, J. Tightly Bound Trions in Monolayer MoS_2. *Nat. Mater.* **2013**, *12*, 207–211.
7. Ross, J. S.; Wu, S.; Yu, H.; Ghimire, N. J.; Jones, A. M.; Aivazian, G.; Yan, J.; Mandrus, D. G.; Xiao, D.; Yao, W.; *et al.* Electrical Control of Neutral and Charged Excitons in a Monolayer Semiconductor. *Nat. Commun.* **2013**, *4*, 1474.
8. Berkelbach, T. C.; Hybertsen, M. S.; Reichman, D. R. Theory of Neutral and Charged Excitons in Monolayer Transition Metal Dichalcogenides. *Phys. Rev. B: Condens. Matter Mater. Phys.* **2013**, *88*, 045318.
9. Kheng, K.; Cox, R. T.; d' Aubigné, M. Y.; Bassani, F.; Saminadayar, K.; Tatarenko, S. Observation of Negatively Charged Excitons X^- in Semiconductor Quantum Wells. *Phys. Rev. Lett.* **1993**, *71*, 1752–1755.
10. Esser, A.; Runge, E.; Zimmermann, R.; Langbein, W. Photoluminescence and Radiative Lifetime of Trions in GaAs Quantum Wells. *Phys. Rev. B: Condens. Matter Mater. Phys.* **2000**, *62*, 8232–8239.
11. Matsunaga, R.; Matsuda, K.; Kanemitsu, Y. Observation of Charged Excitons in Hole-Doped Carbon Nanotubes Using Photoluminescence and Absorption Spectroscopy. *Phys. Rev. Lett.* **2011**, *106*, 037404.
12. Mouri, S.; Miyauchi, Y.; Iwamura, M.; Matsuda, K. Temperature Dependence of Photoluminescence Spectra in Hole-Doped Single-Walled Carbon Nanotubes: Implications of Trion Localization. *Phys. Rev. B: Condens. Matter Mater. Phys.* **2013**, *87*, 045408.
13. Nishihara, T.; Yamada, Y.; Okano, M.; Kanemitsu, Y. Trion Formation and Recombination Dynamics in Hole-Doped Single-Walled Carbon Nanotubes. *Appl. Phys. Lett.* **2013**, *103*, 023101.
14. Park, J. S.; Hirana, Y.; Mouri, S.; Miyauchi, Y.; Nakashima, N.; Matsuda, K. Observation of Negative and Positive Trions in the Electrochemically Carrier-Doped Single-Walled Carbon Nanotubes. *J. Am. Chem. Soc.* **2012**, *134*, 14461–14466.
15. Nish, A.; Hwang, J. Y.; Doig, J.; Nicholas, R. J. Highly Selective Dispersion of Singlewalled Carbon Nanotubes Using Aromatic Polymers. *Nat. Nanotechnol.* **2007**, *2*, 640–646.
16. Bisri, S. Z.; Gao, J.; Derenskyi, V.; Gomulya, W.; Iezhokin, I.; Gordiichuk, P.; Herrmann, A.; Loi, M. A. High Performance Ambipolar Field-Effect Transistor of Random Network Carbon Nanotubes. *Adv. Mater.* **2012**, *24*, 6147–6152.
17. Lee, K. H.; Kang, M. S.; Zhang, S.; Gu, Y.; Lodge, T. P.; Frisbie, C. D. "Cut and Stick" Rubbery Ion Gels as High Capacitance Gate Dielectrics. *Adv. Mater.* **2012**, *24*, 4457–4462.
18. Kim, S. H.; Hong, K.; Xie, W.; Lee, K. H.; Zhang, S.; Lodge, T. P.; Frisbie, C. D. Electrolyte-Gated Transistors for Organic and Printed Electronics. *Adv. Mater.* **2012**, *25*, 1822–1846.
19. Ha, M.; Seo, J.-W. T.; Prabhumirashi, P. L.; Zhang, W.; Geier, M. L.; Renn, M. J.; Kim, C. H.; Hersam, M. C.; Frisbie, C. D. Aerosol Jet Printed, Low Voltage, Electrolyte Gated Carbon Nanotube Ring Oscillators with sub-5 μs Stage Delays. *Nano Lett.* **2013**, *13*, 954–960.
20. Shimotani, H.; Tsuda, S.; Yuan, H.; Yomogida, Y.; Moriya, R.; Takenobu, T.; Yanagi, K.; Iwasa, Y. Continuous Band-Filling Control and One-Dimensional Transport in Metallic and Semiconducting Carbon Nanotube Tangled Films. *Adv. Funct. Mater.* **2014**, *24*, 3305–3311.
21. Xu, F.; Wu, M.-Y.; Safron, N. S.; Roy, S. S.; Jacobberger, R. M.; Bindl, D. J.; Seo, J.-H.; Chang, T.-H.; Ma, Z.; Arnold, M. S. Highly Stretchable Carbon Nanotube Transistors with Ion Gel Gate Dielectrics. *Nano Lett.* **2014**, *14*, 682–686.
22. Tanaka, Y.; Hirana, Y.; Niidome, Y.; Kato, K.; Saito, S.; Nakashima, N. Experimentally Determined Redox Potentials of Individual (n,m) Single-Walled Carbon Nanotubes. *Angew. Chem., Int. Ed.* **2009**, *48*, 7655–7659.
23. Schäfer, S.; Cogan, N. M. B.; Krauss, T. D. Spectroscopic Investigation of Electrochemically Charged Individual (6,5) Single-Walled Carbon Nanotubes. *Nano Lett.* **2014**, *14*, 3138–3144.
24. Weisman, R. B.; Bachilo, S. M. Dependence of Optical Transition Energies on Structure for Single-Walled Carbon Nanotubes in Aqueous Suspension: An Empirical Kataura Plot. *Nano Lett.* **2003**, *3*, 1235–1238.
25. Kang, M. S.; Frisbie, C. D. A Pedagogical Perspective on Ambipolar FETs. *ChemPhysChem* **2013**, *14*, 1547–1552.
26. Zaumseil, J.; Friend, R. H.; Sirringhaus, H. Spatial Control of the Recombination Zone in an Ambipolar Light-Emitting Organic Transistor. *Nat. Mater.* **2006**, *5*, 69–74.
27. Bisri, S. Z.; Takenobu, T.; Sawabe, K.; Tsuda, S.; Yomogida, Y.; Yamao, T.; Hotta, S.; Adachi, C.; Iwasa, Y. P-i-n Homojunction in Organic Light-Emitting Transistors. *Adv. Mater.* **2011**, *23*, 2753–2758.
28. Jo, S.; Ubrig, N.; Berger, H.; Kuzmenko, A. B.; Morpurgo, A. F. Mono- and Bilayer WS_2 Light-Emitting Transistors. *Nano Lett.* **2014**, *14*, 2019–2025.
29. Zhang, Y. J.; Oka, T.; Suzuki, R.; Ye, J. T.; Iwasa, Y. Electrically Switchable Chiral Light-Emitting Transistor. *Science* **2014**, *344*, 725–728.
30. Ghosh, S.; Bachilo, S. M.; Simonette, R. A.; Beckingham, K. M.; Weisman, R. B. Oxygen Doping Modifies near-Infrared Band Gaps in Fluorescent Single-Walled Carbon Nanotubes. *Science* **2010**, *330*, 1656–1659.
31. Miyauchi, Y.; Iwamura, M.; Mouri, S.; Kawazoe, T.; Ohtsu, M.; Matsuda, K. Brightening of Excitons in Carbon Nanotubes on Dimensionality Modification. *Nat. Photonics* **2013**, *7*, 715–719.
32. Piao, Y.; Meany, B.; Powell, L. R.; Valley, N.; Kwon, H.; Schatz, G. C.; Wang, Y. Brightening of Carbon Nanotube Photoluminescence through the Incorporation of sp^3 Defects. *Nat. Chem.* **2013**, *5*, 840–845.
33. Steiner, M.; Freitag, M.; Perebeinos, V.; Naumov, A.; Small, J. P.; Bol, A. A.; Avouris, P. Gate-Variable Light Absorption and Emission in a Semiconducting Carbon Nanotube. *Nano Lett.* **2009**, *9*, 3477–3481.
34. Spataru, C. D.; Léonard, F. Tunable Band Gaps and Excitons in Doped Semiconducting Carbon Nanotubes Made Possible by Acoustic Plasmons. *Phys. Rev. Lett.* **2010**, *104*, 177402.
35. Watanabe, K.; Asano, K. Trions in Semiconducting Single-Walled Carbon Nanotubes. *Phys. Rev. B: Condens. Matter Mater. Phys.* **2012**, *85*, 035416.
36. Mueller, T.; Kinoshita, M.; Steiner, M.; Perebeinos, V.; Bol, A. A.; Farmer, D. B.; Avouris, P. Efficient Narrow-Band Light Emission from a Single Carbon Nanotube p-n Diode. *Nat. Nanotechnol.* **2009**, *5*, 27–31.
37. Hertel, T.; Himmelein, S.; Ackermann, T.; Stich, D.; Crochet, J. Diffusion Limited Photoluminescence Quantum Yields in 1-D Semiconductors: Single-Wall Carbon Nanotubes. *ACS Nano* **2011**, *4*, 7161–7168.

38. Smith, A. M.; Mancini, M. C.; Nie, S. Bioimaging: Second Window for *in vivo* Imaging. *Nat. Nanotechnol.* **2009**, *4*, 710–711.
39. Welsher, K.; Sherlock, S. P.; Dai, H. Deep-Tissue Anatomical Imaging of Mice Using Carbon Nanotube Fluorophores in the Second Near-Infrared Window. *Proc. Natl. Acad. Sci. U. S. A.* **2011**, *108*, 8943–8948.